Carbon Capture Science & Technology 6 (2023) 100095

Contents lists available at ScienceDirect

Carbon Capture Science & Technology

journal homepage: www.elsevier.com/locate/ccst

Full Length Article

Use of copper carbonate as corrosion inhibitor for carbon steel in post combustion carbon capture

Epameinondas Skountzos[a], Cameron A. Price[b,c], Mustafa M. Alsalem[d], Samuel G. Booth[a], Simone Pollastri[e], Serena A. Cussen[f], Christopher M.A. Parlett[b,c,g,h,*], Kyra L. Sedransk Campbell[a,*]

[a] Department of Chemical and Biological Engineering, University of Sheffield, Sheffield, S1 3JD, UK
[b] Department of Chemical Engineering, University of Manchester, Manchester, M13 9PL, UK
[c] UK Catalysis Hub, Research Complex at Harwell, Rutherford Appleton Laboratory, Harwell, OX11 0FA, UK
[d] Department of Chemical Engineering, Imperial College London, South Kensington Campus, SW7 2AZ, UK
[e] Elettra-Sincrotrone Trieste, Strada Statale 14, 34149, Basovizza, Trieste, Italy
[f] Department of Materials Science and Engineering, University of Sheffield, Sheffield, S1 3JD, UK
[g] Diamond Light Source, Harwell Science and Innovation Campus, Didcot OX11 0DE, UK
[h] The University of Manchester at Harwell, Diamond Light Source, Harwell Science and Innovation Campus, Didcot OX11 0DE, UK

ARTICLE INFO

Keywords:
Corrosion
Amines
Carbon Capture
Copper Carbonate Basic
Inhibition
CO_2

ABSTRACT

The realisation of post-combustion CO_2 capture (PCCC) at industrial scale remains limited; one challenge is the concerns around capital costs and another concern is corrosion of the system itself. Corrosion resistance and mitigation against the amine solvent monoethanolamine (MEA) was studied, using the inhibitor copper (II) carbonate basic (CC). Carbon steel (C1018) was tested in CO_2 loaded, 5M aqueous MEA solution, alone and in the presence of CC, to assess the corrosivity of the solution. Immersion testing used mass loss, Fe and Cu ion concentration in solution *via* ICP-MS, imaging (SEM) and analytical techniques (XRD and EDX) to investigate the effect of corrosion. Generally, the use of CC improved C1018 corrosion resistance relative to C1018 alone. Even at low concentrations (0.9 mM), CC was effective in inhibiting corrosion against CO_2 loaded MEA, as the observed corrosion rate was effectively zero and no dissolved Fe was detected in solution. There was no evidence of copper surface adsorption. To clarify the solution chemistry resulting in corrosion inhibition, the local chemical environment of Fe and Cu were probed by Cu and Fe K-edge X-ray Absorption Spectroscopy, respectively. The Cu K- edge HERFD-XANES spectra reveal that a Cu^{2+} amine complex forms, critical to understanding the structure which is promoting significant corrosion inhibition.

Introduction

Emissions of greenhouse gasses, including carbon dioxide (CO_2), have resulted from our global economic development whilst simultaneously causing adverse effects on our environment (Cozzi et al., 2021, Stowe and Hwang, 2017). Changing weather patterns, including increasing volatility and rising sea levels are two globally catastrophic impacts that demonstrate the imperative in implementing climate change mitigation strategies. With a majority of CO_2 emission from fossil fuel and industrial processes, the capture and subsequent removal from these CO_2 point sources is imperative (Khatri et al., 2006, MacDowell et al., 2010, Wu et al., 2014). Post-combustion carbon capture (PCCC), employing amine scrubbing, is a promising technology to capture CO_2 from a pure or mixed gas steam, which can then be transported *via* pipeline, to storage sites (Haszeldine, 2009). Amine scrubbing is a mature technology that is derive from natural gas sweetening where acid gases, namely CO_2 and H_2S, are removed using aqueous amine solutions (Rochelle, 2009, Kittel et al., 2009). Although amine-based carbon capture is the most advanced solution to our emissions problem, limitations pertaining to corrosion remain a key obstacle against deploying this technology.

Amine solvents are not intrinsically corrosive (Alvis et al., 2015), by contrast, aqueous amine solutions, when exposed to CO_2, degrade and become corrosive (DuPart et al., 1993). The corrosivity of the aqueous amine solutions in PCCC is mostly attributed to the presence of acid gases, presence of impurities from the flue gas (*e.g.* O_2, NO_x and SO_x), degradation products resulting from reactions due, in part, to the impurities in the flue gas and metal ions (Mondal et al., 2012, Zheng et al., 2016). This issue leads to significant risks as well as high maintenance

* Corresponding authors.
E-mail addresses: christopher.parlett@manchester.ac.uk (C.M.A. Parlett), k.sedransk@sheffield.ac.uk (K.L. Sedransk Campbell).

https://doi.org/10.1016/j.ccst.2022.100095
Received 19 October 2022; Received in revised form 22 December 2022; Accepted 23 December 2022

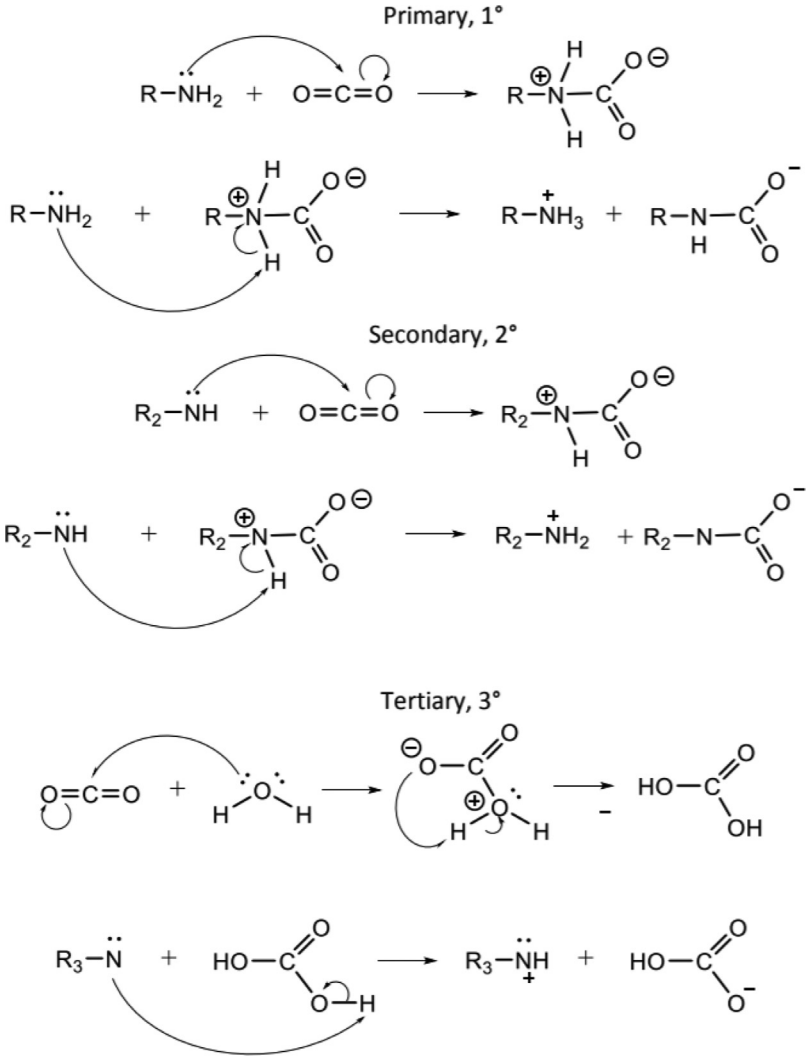

Fig. 1. CO_2 mechanism of primary, secondary and tertiary amines (Yu, 2015).

costs if carbon steel is used; with stainless steels however, all risk is not removed and dramatically elevated construction costs are incurred, alongside additional operational costs to deploy suitable risk management strategies (Gunasekaran et al., 2013, Campbell et al., 2017). As such, the combination of safety and financial concerns due to corrosion are significant hurdles towards wider implementation of PCCC. So far, studies on carbon steel (a cheaper and therefore financially more desirable solution) have demonstrated the material's susceptibility to corrosion, only a limited number of mitigation technologies have been proposed. Two approaches have been touted as corrosion countermeasures, either selection of less corrosive amine solutions (Zheng et al., 2016, Campbell et al., 2017, Zheng et al., 2016) and/or the use of inhibitors (Zheng et al., 2015, Sadeek et al., 2018).

The implementation of appropriate mitigation strategies against corrosion must target the causes of corrosion appropriately. Generally, primary (1°) and secondary (2°) amines undergo a mechanism of 'direct' CO_2 uptake (Fig. 1). By contrast, tertiary (1°) and sterically hindered (does not have to be tertiary) undergo an 'indirect' CO_2 uptake mechanism (Kohl and Nielsen, 1997).

The current benchmark solvent is the 1° amine, monoethanolamine (MEA), at 30 wt.% concentration, due to its fast CO_2 uptake kinetics. However, it has extensive limitations including low CO_2-uptake capacity and susceptibility to both thermal and oxidative degradation. In 1° amines, the formation of carbamate in the reaction pathway intensifies corrosion (Xiang et al., 2014). The capture mechanism leads to carbamate formation, which is adsorbed to the steel surface thereby leading enhancing the corrosiveness of amines (Mondal et al., 2012).

Although not discussed in detail here, 3° amines, by contrast, generate carbonate ions which react with oxidised surface Fe^{2+} to form a protective layer of $FeCO_3$ (Campbell et al., 2017, Zheng et al., 2016). However, the drawbacks to the use of 3° amines makes interest in their deployment alone less popular.

Given the propensity of aqueous amine PCCC systems to exhibit corrosion, a surprisingly few studies have been focused on preventive measures. Cathodic protection, anti-corrosive coatings and corrosion inhibitor injection are the three most notable approaches cited (Uhlig and Revie, 2008). Corrosion inhibitors are, strategically and economically, an ideal option given that little to no modification of the existing PCCC plant process is required.

Corrosion inhibitors are chemical additives that react with metal surface or bulk environment to decrease the observed corrosion rate on the infrastructure material. The corrosion inhibitor effectiveness depends on the type and concentration of inhibitor, molecule structure, nature of metal surface as well as other process parameters (*e.g.* operating temperature) (Desimone et al., 2011). Inhibitors are primarily classed in environmental modifiers, that interact with the aggressive species in solution, and inhibitors absorbed to the metal surface. Depending on which reaction the inhibitor is supressing, they are further classified in cathodic, anodic and mixed inhibitors (Aliofkhazraei, 2018). To experimentally determine the effectiveness of a given inhibitor, the mass loss

Table 1
Survey of corrosion inhibitors used in amine scrubbing plants.

System	Inhibitor used
65% MEA + CO_2, Mild steel (Mago and West, 1976)	0.05% sodium metavanadate ($NaVO_3$) 0.05% potassium antimonyl tartrate ($C_8H_{10}K_2O_{15}Sb_2$) 0.05% stannous tartrate ($C_4H_4O_6Sn$)
50% DEA + H_2S/CO_2 ratio 9/1 (Holoman et al., 1978)	(i) 1000 ppm Polyethylene polyamine (PEI) (ii) PEI + Copper carbonate ($CuCO_3$) (iii) PEI + $CuCO_3$+S (iv) Polyethylene polyamine (E-100) (v) E-100 + $CuCO_3$ (vi) E-100 + $CuCO_3$+PEI
30% MEA + CO_2 + 100-500 ppm of H_2S, Mild steel (Asperger et al., 1979)	Quaternary pyridinium salt, lower alkylenepolyamine (ethylene or propylene polyamine) or polyalkylene polyamine
30% MEA + saturated CO_2, Mild steel (Clouse and Asperger, 1978)	1-tertradecyl alkylpyridinium salt, thioacetamide (C_2H_5NS) and cobalt acetate ($Co(CH_3COO)_2$)
35% MEA, CO_2 + >500 ppm of H_2S, Mild steel (Clouse and Asperger, 1978)	Tetradecylalkylpyridinium bromide, ammonium thiocyanate (NH_4SCN) and cobalt acetate ($Co(CH_3COO)_2$)
80% MEA + saturated H_2S at 25°C, Mild steel (Asperger et al., 1979)	Copper compounds ($CuCO_3$, CuS) + an Oxidizer ($KMnO_4$)
50% MEA + 0.39 CO_2 loading (Nieh, 1983)	(i) Ethylene diamine ($C_2H_8N_2$) + Vanadium (ii) Propylene diamine ($C_3H_{10}N_2$) + Vanadium (iii) N-aminoethylpiperazine + Vanadium
30% MEA + saturated CO_2, 304 Stainless steel (Oakes et al., 4452764)	Trivalent bimuth (Bi) compounds
30% MEA + saturated CO_2 at 250°C, AISI 1020, AISI 304, AISI 33116 and Monel (DuPart et al., 1984)	Ammonium thiocyanate (NH_4SCN), nickel sulfate ($NiSO_4$) and bismuth citrate
30% MEA+ saturated CO_2 + 4-7% O_2, Mild steel (Pearce and Pauley, 4440731)	Copper carbonate ($CuCO_3$) + dihydroxyethylglycine
25% MEA, 5% hydroxyethylethylene-diamine, 70% water, CO_2 and H_2S, 1020 Mild steel (Jones and Alkire, 1985)	Quaternary pyridine salt, a surface-active agent and/or a thio-compound and a water-soluble nickel compound
30% MEA + CO_2 + H_2S, Mild steel (McCullough and Barr, 1985)	Vanadium compounds and organic compound (nitro substituted aromatic acids)
30% MEA+ CO_2 saturated, 140°C (Henson et al., 1986)	Thiourea-aminopiperazinefomaldehyde + nickel (II) salts

of a metal coupon (placed in the process) is monitored, where the difference between the uninhibited ($CR_{uninhibited}$) and inhibited ($CR_{inhibited}$) corrosion rate is established (Eq. 1) (Kittel et al., 2009).

$$Inhibitor\ Efficiency\ (\%) = 100 \times \left(CR_{uninhibited} - CR_{inhibited}\right)/CR_{uninhibited} \quad (1)$$

Strong performances of historical inorganic inhibitors on mild steel *e.g.* arsenic, vanadium, in 15-30% MEA solutions at temperatures above 80°C, present challenges due to their toxicity (Saiwan et al., 2011); others present operational difficulties (*e.g.* quarternary pyridinium compounds cause foaming in MEA, DEA, MDEA and AMP) (Thitakamol and Veawab, 2008); and many have added costs due to solvent handling and disposal requirements (Soosaiprakasam and Veawab, 2008). Sodium metavanadate ($NaVO_3$) presents an excellent example of this delicate balance, as exhibited on 1020 carbon steel. $NaVO_3$ was reported to have an inhibition efficiency of 97% in 3M MEA test solutions at 80°C and 1000 ppm inhibitor loading (Veawab et al., 2001), as well as being highly toxic and intensifies MEA degradation (Bello and Idem, 2006). More widely, the performance of many of these cathodic inibitors comes from natural gas sweetening applications (Table 1). As such, interest is shifting away from inorganic inhibitors, that mostly function as anodic inhibitors offering metal passivation, to low-toxic and/or organic inhibitors when looking towards PCCC technology (Veawab et al., 2001).

Whilst only a limited number of studies have been conducted to explicitly address the challenges of identifying reasonable corrosion inhibitors for PCCC, three approaches have been used to intelligently target the cause of corrosion (Table 2). The three strategies are: (1) anodic protection, (2) cathodic protection and (3) increased viscosity.

Cathodic protection is the most widely used corrosion mitigation technique and consists of passivating the metal surface, by converting it to a cathode. Cathodic protection is achieved by the sacrificial anode method or the impressed current cathodic protection (Aliofkhazraei, 2018). Anodic protection is offered when a surface is treated by anodic polarisation, which causes the formation of a passive film. In order to achieve anodic protection, it is necessary to maintain the passivation potential at all times. Lastly, in the case of using ionic liquids as inhibitors, the viscosity increase corresponds to a decrease in corrosion rate as the slow diffusion of oxidizing species suppresses the kinetics of corrosion (Hasib-Ur-Rahman and Larachi, 2013).

The less toxic copper (II) carbonate basic ($CuCO_3Cu(OH)_2$, CC) showed satisfactory performance with inhibition efficiency of 80% but might induce some pitting corrosion in absence of O_2. However, the performance is worsened by degradation products (Soosaiprakasam and Veawab, 2009). Sodium thiosulfate ($Na_2S_2O_3$, STS) showed effective inhibition (up to 94%). Electrochemical study showed that the inhibitor was anodic and produced instable passive film of thiosulfate ($S_2O_3^{2-}$) ions adsorption that retards corrosion (Srinivasan et al., 2013). 2-Mercaptobenzimidazole (MBI) significantly increases the polarization resistance of the aqueous solution and inhibits the corrosion. Even though no protective layer was detected, it is predicted that thin and porous protective layer of MBI might cover the metal surface. However, fast degradation at high temperature and the formation of FeS layer with stress cracking suggests that MBI may not be suitable for PCCC (Zheng et al., 2015).

The work reported herein assesses the performance of CC inhibited carbon steel 1018, relative to uninhibited carbon steel, in 5M MEA solutions loaded with CO_2. The test conditions are simulating high temperature processes found in PCCC. This industrially relevant study aims to understand (1) the performance of CC as a corrosion inhibitor in the benchmark amine solvent, (2) the mechanism of inhibition exhibited

Table 2
Carbon steel corrosion inhibition studies in aqueous amine systems.

MEA concentration	Temperature (°C)	CO_2 loading ($^{mol CO_2}/_{mol MEA}$)	Inhibitor	Inhibitor efficiency (%)	Corrosion rate	Mechanism
5, 7 and 9 M (Soosaiprakasam and Veawab, 2009)	40 and 80	0.2 and 0.55	50-500 ppm copper carbonate	>80	<0.254 mmpy	Anodic inhibitor
3 M (Veawab et al., 1997)	80	Saturated	100 ppm aliphatic amine 1000-5000 ppm carboxylic acid 1000 ppm sulfoxide	75-92 (carboxylic acid > sulfoxide > amine)	-	Cathodic inhibitor
			1000 ppm sodium metavanadate	97		Anodic inhibitor
5 M (Zheng et al., 2015)	108	0.43	5 mM MBI	-	15.9 g m^{-2} d^{-1} 14.9 g m^{-2} d^{-1}	Mixed inhibitor
5 M (Srinivasan et al., 2013)	80	0.55	250-10000 ppm sodium metavanadate	91-94	0.26 – 0.38 mmpy	Anodic inhibitor
10 wt. % (Acidi et al., 2014)	25	0.4	3 wt. % [emim][BF_4]	99.8	0.22 mpy	Increased viscosity
			3 wt. % [emim][Otf]	97.6	2.65 mpy	
30 wt. % (Hasib-Ur-Rahman and Larachi, 2013)	25	0.35	10 wt. % [emim][Otf]	42	11.24 mpy	Increased viscosity
			10 wt. % [emim][DCA]	-3	19.85 mpy	
			10 wt. % [emim][acetate]	61	7.51 mpy	
			10 wt. % [emim][tosylate]	28	13.8 mpy	
			30 wt. % [emim][Otf]	44	10.8 mpy	
			30 wt. % [emim][DCA]	44	10.74 mpy	
			30 wt. % [emim][acetate]	88	2.29 mpy	
			30 wt. % [emim][tosylate]	58	8.11 mpy	

by CC and (3) the solution chemistry and potential species formed as a result of CC loading. Since amines are employed in various industrial applications, such as natural gas sweetening, this study has even wider implications.

Materials and methods

Corrosion experiments

Three sets of experiments were performed in this study. Initially, to evaluate the corrosion behaviour of carbon steel in CO_2 loaded MEA, a set of corrosion experiments was performed by immersing carbon steel coupons in 5 M MEA at 60 °C for one, five and ten weeks. The behaviour of steel in the corrosion tests was used as a baseline to assess the inhibitors performance in subsequent experiments. The inhibition of corrosion tests were performed by immersion of carbon steel coupons in 5 M MEA at 60 °C, containing 0.9, 2.3, 4.5 and 9.0 mM copper carbonate, in all cases for 13 weeks. Finally, to examine the behaviour of copper carbonate in an aqueous amine solution and study the bulk chemistry and possible complexation, a set of experiments was performed where CC was added to CO_2 loaded MEA and samples were taken every ten minutes for a total duration of 120 minutes, to study the dissolution process of the inhibitor.

The experimental procedure followed has been previously explained (Sadeek et al., 2018, Alsalem et al., 2021). Initially, 152.7 g of MEA was weighted on a precision scale (Denver Instrument) in a 500 mL volumetric flask prefilled with 100 mL DI water and then further diluted with DI water to produce a total volume of 500 mL. The solution then was transferred into two 250 mL round bottom flask using a graduated cylinder. In all experiments, 250 mL borosilicate glass round bottom flask, with a reflux condenser (to minimise vapour losses) were used on heating blocks (with a bespoke aluminium plate to enhance heat transfer). After transfer, the solutions were purged with nitrogen (N_2) for one hour (≥100 mL min^{-1}, fixed with using a digital flow meter, Agilent ADM-1000) at ambient temperature and pressure, to remove dissolved oxygen and minimise possibility of amine oxidative degradation. Subsequently, CO_2 was loaded at 20 mL min^{-1} for two hours and then the duration of the experiment. The temperature was set to 60.0 °C to fall within the range of 40-80 °C of the PCC process (absorber, heat exchanger, lowest end of stripper).

Carbon steel (C1018, 76.2 mm x 9.5 mm x 1.6 mm) coupons (Table 3) had glass bead blasted finish and were washed thoroughly with DI water and acetone to remove any surface debris, dried and weighed with a precision scale. The coupons were immersed in the loaded solutions and upon termination of the experiment, they were removed gently dried and weighed again. The net mass loss in percentage was calculated by Eq. 2.

$$Net\ mass\ loss\ (\%) = \frac{m_{initial} - m_{final}}{m_{initial}} \times 100 \quad (2)$$

Corrosion rates in mm per year (mmpy) were calculated by the difference in mass before and after immersion, divided by metal coupon density, ρ, exposed surface area, A, and immersion time in years, t, as shown in Eq. 3.

$$Corrosion\ rate\ (mmpy) = \frac{\left(m_{initial} - m_{final}\right)}{A \times t \times \rho} \quad (3)$$

Analytical techniques

Post immersion, Fe and Cu concentration were measured in triplicate using Inductively Coupled Plasma – Mass Spectroscopy (7900, Agilent Technologies). Surface imaging was performed using Scanning Electron Microscopy (JSM 6400, Jeol) where the samples had been coated with 10 nm of Au using a sputter coater (K575X, Quorum Technologies). The Energy Dispersive X-ray Spectroscopy detector was used for elemental analysis and was calibrated using a Co standard. Powder X-ray diffraction measurements of the coupons were measured using an X'Pert (PANalytical) across a 2θ range of 20° to 110° (step size 0.0334°, scan rate 6° min^{-1}).

X-ray absorption spectroscopy (XAS) studies

Cu and Fe K-edge High Energy Resolution Fluorescence Detected X-ray Absorption Near-Edge Spectroscopy (HERFD-XANES) were collected at Diamond Light Source, UK, on beamline I20 scanning (Diaz-Moreno et al., 2018), using a Si (111) four-bounce monochromator calibrated at the energy of the Cu and Fe K edges with metal foils. HERFD-XANES were collected using a Johann-type spectrometer equipped with either three Ge (440) for Fe or Si (444) for Cu crystal analysers and a medipix detector. The spectrometer energy was focused at 6404 or 8048 eV for Fe and Cu, corresponding to the Kα_1 maximum intensity for the two elements, with the emission spectrometer purged with He.

Table 3
Chemical composition of C1018 steel coupons (Alabama Coupons).

Element	C	Mn	P	S	Si	Cu	Ni	Cr
Weight %	0.180	0.800	0.021	0.004	0.280	0.140	0.040	0.050
Element	Mo	Al	Nb	V	Ti	N	Ca	Sn
Weight %	0.010	0.035	0.002	0.001	0.001	0.007	0.002	0.006

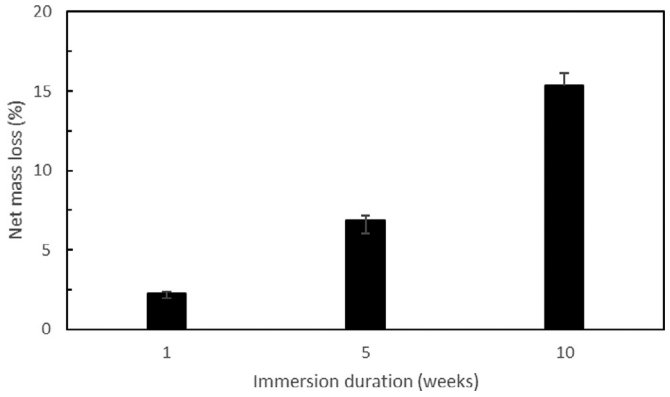

Fig. 2. Net mass loss in percentage of C1018 coupons exposed to CO_2 loaded MEA solutions at 60 °C for 1, 5 and 10 weeks.

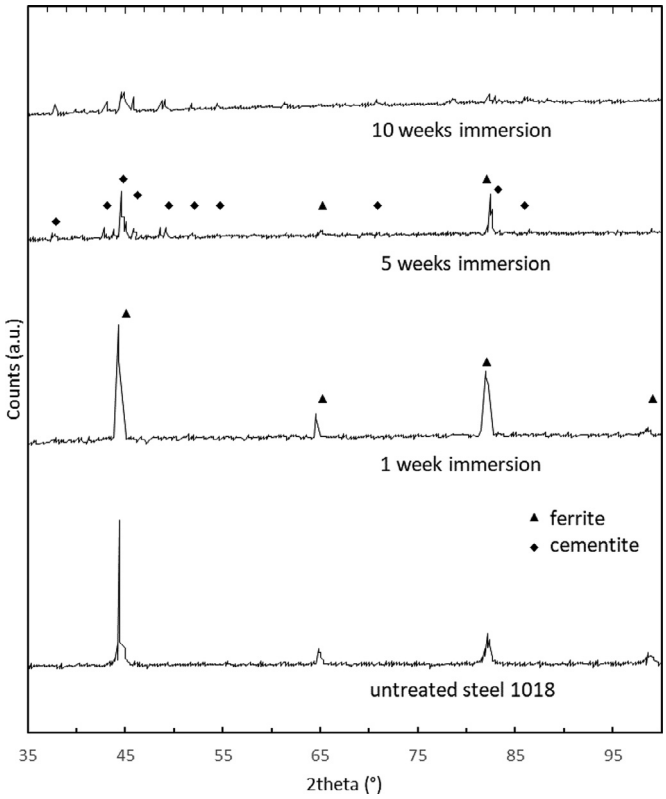

Fig. 3. XRD patterns of C1018 coupons exposed to CO_2 loaded MEA solutions at 60 °C for 1, 5 and 10 weeks. The standard peaks of the phases identified are displayed.

HERFD-XANES were collected on liquid samples using a previously reported liquid recirculating configuration (Parlett et al., 2014), to minimise beam damage. This comprised a 6 mm ID Kapton tube, as a measurement cell, connected via PTFE tubing to a 25 mL two-necked round bottom flask reservoir, with the recirculating solution pumped by a peristaltic pump. The solution reservoir was situated in a temperature-controlled, stirred oil bath, with temperatures between 25-80°C for *in situ* temperature studies.

Spectra were processed using IFEFFIT (v1.2.12) open-source software suite, with Athena (v0.9.26) for the normalisation, background subtraction and linear Combination Fitting (LCF) of HERFD-XANES spectra. Solid references of Fe_2O_3, Fe_3O_4, $Fe(NO_3)_3{\cdot}9H_2O$, FeO, FeO(OH), Cu_2O $Cu_2(OH)_2CO_3$, $Cu(NO_3)_2{\cdot}3H_2O$, CuO, $Cu(OH)_2$ and $[Cu(NH_3)_4]SO_4{\cdot}H_2O$ were collected alongside liquid references of CC dissolved in 5M MEA and 5M Isobutylamine.

Results and discussion

Carbon steel corrosion in CO_2 loaded MEA

A combination of techniques was used in this study to identify and quantify the corrosion behaviour of carbon steel in aqueous CO_2 loaded MEA solutions. Three approaches were recorded to establish the corrosion behaviour: (1) changing mass of the coupon, (2) recovery of solid product from the vessel (e.g. from the walls), (3) concentration of Fe in solution. The net mass change (Eq. 2) reported represents the changing mass of the immersed coupon (Fig. 2), where an increasing mass loss is observed as a function of increasing time.

The XRD patterns of initial C1018 coupons indicate ferrite, as expected (Fig. 3). The mass loss measured (Fig. 2), can be explained by XRD analyses made after one, five and ten weeks of immersion. After one week of immersion little difference is observed (Fig. 3). However, there is an increasing presence of cementite (Fe_3C) with increasing immersion time to five and then ten weeks. The more labile Fe found in ferrite is removed, resulting in the exposure of cementite. After ten weeks cementite is dominant at the surface and near surface depths probed by XRD. Additionally, analysis of the collectible mass revealed relatively amorphous samples with peaks corresponding to magnetite (Fe_3O_4) and goethite (α-FeOOH) (Figs. I-III in Supplementary Information).

It should be noted that the collectible mass for those three experiments were larger in mass than the corresponding net mass losses, which raises the question of closing the Fe mass balance *i.e.* how much Fe dissolved vs how much Fe is in solution and/or precipitated. This behaviour can be explained by Fe ions forming compounds with amine species and eventually precipitating on the vessel walls once the saturation limits have been exceeded.

Imaging of the untreated C1018 coupons indicate a smooth surface (Fig. 4A), where EDX analysis indicated the presence of Fe and nominal C. After one week of immersion in CO_2 loaded MEA solution (Fig. 4B), changes to the surface are immediately apparent; the surface has an increase in apparent roughness as well as flat regions. Analysis of the rough regions showed significant increases in carbon, from nominal before immersion to contents *ca.* 50-60 at.%. This dramatic increase can be attributed to exposure of iron carbide (Fe_3C), a component of the pearlite microstructure found in carbon steel. The flat regions show a similar concentration profile (containing primarily Fe, with traces of C and Mn) to the sample before immersion. After five weeks of immersion (Fig. 4C), most of the corroded surface appears rough with smooth areas now only minimally present.

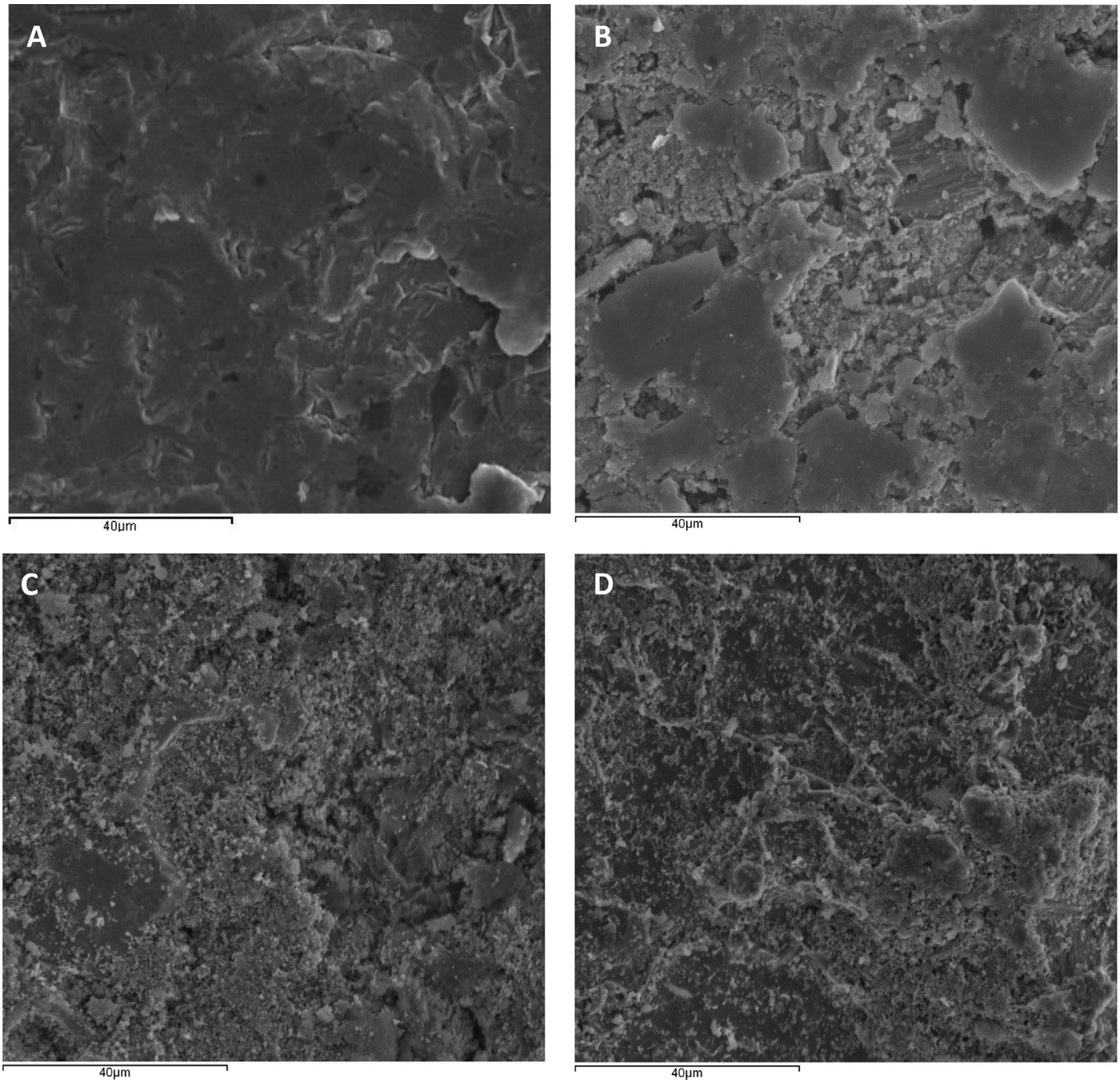

Fig. 4. SEM imaging of (A) untreated C1018 coupons and exposed to CO_2 loaded MEA solutions at 60 °C for (B) 1, (C) 5 and (D) 10 weeks.

The apparent roughness is evolving from that seen after one week, where deposited and/or growing corrosion products are present. Whilst not obvious on SEM, due to the presence of scale (*i.e.* corrosion products), extensive pitting was also observed in optical microscopy imaging (Fig. IV in Supplementary Information). The few remaining smooth surfaces continue to show a composition of the C1018 alloy. The corrosion products observed, often round clusters and elongated crystals, contain Fe, C and O; the combination of these elements suggests iron oxide (FeO, Fe_3O_4) and iron carbide (Fe_xC_y). The appearance of the products suggest that $FeCO_3$ is not notably present.

After ten weeks of immersion (Fig. 4D), imaging shows a significantly damaged surface, which could be described as porous, where coupons are suffering from severe pitting as well as general corrosion behaviours (Fig. IV in Supplementary Information). Elemental analysis, by EDX, identified the severely damaged regions to have high concentrations of Fe and C; however, only relatively low concentrations, as compared to five weeks, were measured for O (*ca.* 3 at.%). As such, the iron carbide structures clearly are now dominant, with a decrease in the presence of iron oxides. The absence of corrosion products suggested that the corrosion product layers identified prior with SEM had been removed or dissolved.

The analysis of the solid coupon indicates an initial exposure to the CO_2-loaded aqueous amine solution, resulting in the oxidation of Fe. In particular, the labile Fe from ferrite is preferred exposing increasing amounts of cementite. The initial increase in Fe concentration measured in solution after one week of immersion in solution is consistent with this explanation. After one week of immersion (n=3) an Fe concentration of 182 ± 12 mg L^{-1} was measured (Fig. 5A). Between this initial exposure

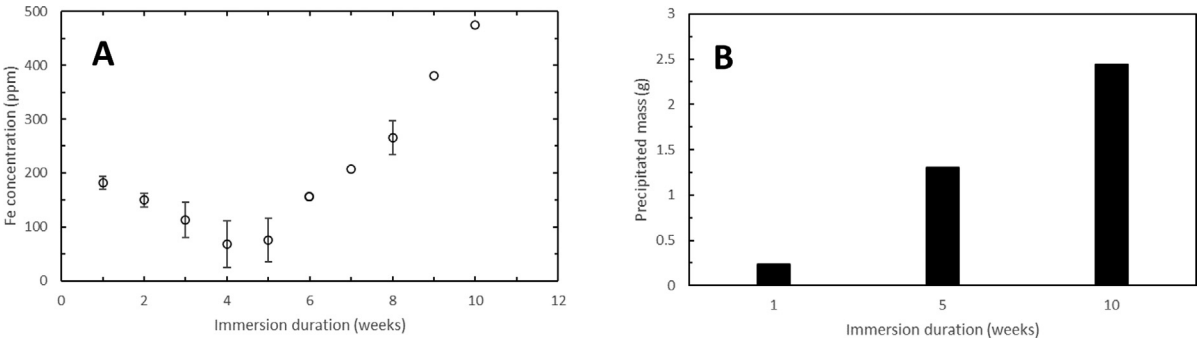

Fig. 5. (A) Concentration of dissolved Fe in solution (identified by ICP-MS) and (B) precipitated mass collected from vessel of 5 M MEA at 60 °C, after 1, 5 and 10 weeks of immersion. Some error bars are too small to be observed.

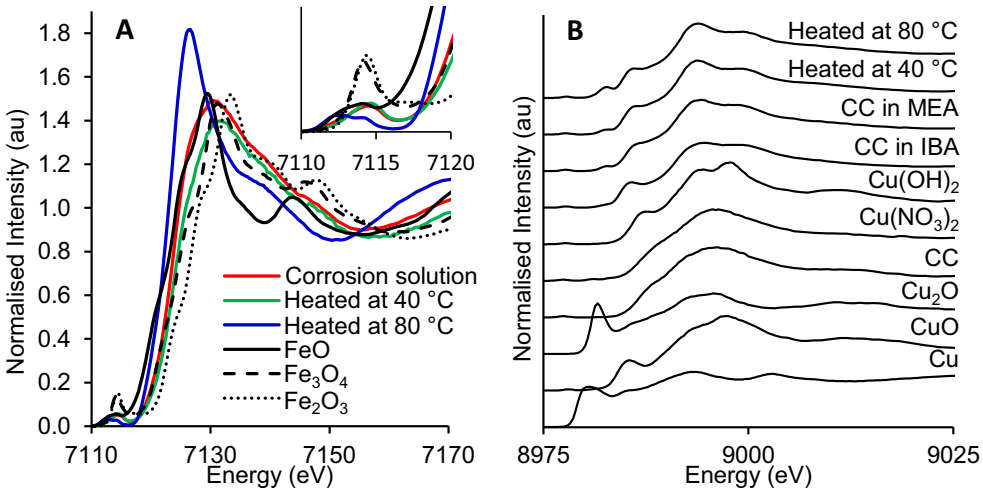

Fig. 6. (A) Fe K edge HERFD-XANES plot of Fe corrosion solution for steel coupon treatment in 5M MEA for 12 weeks, oxide reference standards run as solids and corrosion solution at elevated temperature. (B) Artificially offset stacked Cu K edge HERFD-XANES plot of copper reference spectra run as solids (CC = $Cu_2(OH)_2CO_3$) shown with CC dissolved in IBA and MEA at room temperature and elevated temperatures.

period and the subsequent four weeks, however, a range of behaviours are occurring. There is a continuing oxidation from the surface, whilst simultaneously there is the formation of corrosion products, particularly iron oxides. The formation of these are likely predominantly amorphous, as they are not observed by XRD but are strongly evident by SEM and EDX.

In solution, over these subsequent three weeks, a decreasing concentration was measured with a minima in concentration reached in week 4 (68 ± 44 mg L^{-1}). During this period a substantial portion of the Fe in solution is forming iron oxide which is either depositing on the coupon surface itself or on other available surfaces, *i.e.* the glass walls of the vessels (Fig. 5B).

After four weeks, an increasing Fe concentration in solution was steadily observed through the remaining six weeks which were measured. The final concentration measured is a maxima within the experimental period covered bur shows no indication that it is a plateau. This increasing concentration in solution is the result of continuing Fe oxidation from the surface which is actively corroding. Additionally, it would be expected that due to the amorphous nature of the iron oxide dissolution and re-precipitation would continue to occur.

Inhibition of carbon steel corrosion in CO_2 loaded MEA

The carbon steel coupons immersed in CO_2 loaded MEA, in the presence of CC, exhibited negligible corrosion. In all CC concentrations, the coupons lost very little mass, resulting in an estimated inhibition efficiency above 99.9% (see Table I Supplementary Information). The net mass loss was less than 0.010 % in all cases, suggesting that CC is a promising candidate for inhibiting carbon steel corrosion by CO_2 loaded amines. The successful inhibition was further verified by the ICP-MS analysis, which revealed no traces of Fe in solution, in any of the cases. Moreover, no mass was collected from the vessels post-immersion, suggesting that no precipitation took place during the 13 weeks of immersion. It can be assumed that a minimum inhibitor loading of 0.9 mM is an appropriate corrosion mitigation strategy in a PCC process.

XAS studies

The XAS was deployed to shed light on the nature of Fe speciation from steel coupon corrosion and dissolved Cu inhibitor species. Fe K-edge HERFD-XANES (Fig. 6, Fig. V in Supplementary Information), illustrate that the soluble corrosion species are not oxide (rust) species, note this is solely an analysis of the soluble Fe species. In addition, the Fe species in MEA at room temperature do not resemble any other potentially expected species, including nitrates and oxide-hydroxides. Furthermore, LCF results (Fig. V in Supplementary Information) ruled out the possibility of a physical mixture of these species being present.

The corrosion species spectra display a weak pre-edge feature at 7114.1 eV and edge position at 7123.6 eV, the latter suggesting either a Fe^{2+} or mixed (Fe^{2+} and Fe^{3+}) oxidation state based on the oxide standards. Pre-edge features in first-row transition metal are commonly used to discern structural geometry. However, similar features have been reported for various structures, including distorted tetrahedral Fe complexes (Burkhardt et al., 2017), diiron complexes (Cutsail et al., 2020) and oxide nanoparticles (NP) (Lafuerza et al., 2020). In the case of Fe_3O_4 NPs, the edge and XANES match the bulk oxide (Fe_3O_4), with only a slight shift, thus, we are confident this species is not present here. Upon subjecting the corrosion solution to elevated temperatures (80°C), akin to those used during CO_2 release and MEA regeneration, a second pre-edge feature at 7112.4 eV and an increase in white line intensity are

apparent. The shape, splitting, and intensities of the pre-edge feature is consistent with both octahedral (Lafuerza et al., 2020) and diiron (Cutsail et al., 2020) Fe^{2+} complexes, with edge position and XANES feature appearing comparable.

The Cu K edge HERFD-XANES (Fig. 6B) of the inhibitor solution shows that the dissolved Cu species do not resemble common copper compounds, such as oxides, nitrates or hydroxides, and is distinctly different from the parent salt, copper (II) carbonate hydroxide. However, the inhibitor solution closely matches the spectra of $Cu_2(OH)_2CO_3$ dissolved in isobutylamine (IBA), with an edge position consistent with CuO. Therefore, we confidently proposed a Cu^{2+} amine complex as the inhibitor species, which shows good thermal stability.

The inhibitor spectrum exhibits several features: 1) a pre-edge feature at 8977.7 eV; 2) a low energy rising edge feature at 8982.8 eV; 3) a high energy rising edge feature at 8986.1 eV and 4) a peak maximum above the adsorption edge at 8993.9 eV. The position of these features is comparable to the previously reported spectra for a Cu^{2+} quinoline-amine complex, which displays similar pre-edge, rising edge and XANES features, with respect to intensity and position, with the complex reported to possess a distorted square planar geometry (Vollmers et al., 2016). Closer inspection of the rising edge feature and XANES regions reveal an increase in definition and intensity with heating, which have been attributed to an increase in coordination number and coexistence of a degree of Cu^{1+} respectively (Pappas et al., 2019). Thus the inhibitor complex may display some subtle rearrangement and reduction during the regeneration process of MEA, which could explain decreasing performance over prolonged capture and release cycles.

Conclusions

The potential for the use of CC as a corrosion inhibitor in processes with carbon steel in 5M MEA has been demonstrated. Uninhibited C1018 coupons exhibited high corrosion susceptibility and the formation of Fe-rich species was observed in solution. Moreover, in the case of uninhibited systems, the coupons post immersion are severely corroded, resulting in significant net mass loss. The use of CC in inhibition tests shows an outstanding resistance to corrosion since the corrosion rate became effectively zero and no dissolved Fe is detected in the MEA solution. However, there is no clear evidence of copper adsorption on the coupon surface when examined post immersion. To clarify the solution chemistry under inhibited conditions, the local chemical environment of Fe and Cu were probed by Cu and Fe K-edge HERFD-XANES, respectively. The Fe K-edge spectra confirm corrosion species in solution are not simple oxides, nor a mixture of these. The Cu-K edge XANES spectra reveals that a Cu^{2+} amine species complex (possibly with monodendate ligand of MEA, as observed in the case of isobutylamine), is high likely as the Cu species in solution, thus offering key insights into the structural requirements for an effective corrosion inhibitor.

Declaration of Competing Interest

The authors declare no competing financial interest.

Acknowledgments

The research team would like to acknowledge Nutnicha Manee's contribution to the early related work. KLSC acknowledges the support of the EPSRC and Royal Society for her Dorothy Hodgkin Research Fellowship and the UKCCSRC for the Flexible funding supporting this research. MMA acknowledges the support of Saudi Aramco for his PhD studentship. CAMP and CAHP would like to thank the Research Complex for access and support to these facilities and equipment, and the University of Manchester for funding under the FSE Covid Research Recovery Fund. We acknowledge Diamond Light Source for time on I20-scanning under proposal SP25542.

Supplementary materials

Supplementary material associated with this article can be found, in the online version, at doi:10.1016/j.ccst.2022.100095.

References

Acidi, A., Hasib-ur-Rahman, M., Larachi, F., Abbaci, A., 2014. Ionic liquids [EMIM][BF4], [EMIM][Otf] and [BMIM][Otf] as corrosion inhibitors for CO2 capture applications. Korean J. Chem. Eng. 31, 1043–1048.

Aliofkhazraei, M. *Corrosion inhibitors, Principles and Recent Applications*. (2018). doi:10.5772/intechopen.70101, https://www.intechopen.com/books/6402.

Alsalem, M.M., Camilla, S., Ryan, M.P., Sedransk Campbell, K., 2021. Understanding the role of NaCl concentration on the corrosion of carbon steel and $FeCO_3$ Formation in CO2-containing electrolytes. Ind. Eng. Chem. Res. 60, 12032–12048.

Alvis, R.S., Hatcher, N., Jones, C.E., 2015. Predicting corrosion rates in amine and sour water systems. In: American Fuel and Petrochemical Manufacturers, AFPM - AFPM Annual Meeting 2015, pp. 809–817.

Asperger, R. G., Krawczyk, L. S., Oakes, B. D., 1979. Method and composition for inhibiting the corrosion of ferrous metals. United States Patent 4143119.

Bello, A., Idem, R.O., 2006. Comprehensive study of the kinetics of the oxidative degradation of CO_2 loaded and concentrated aqueous monoethanolamine (MEA) with and without sodium metavanadate during CO_2 absorption from flue gases. Ind. Eng. Chem. Res. 45, 2569–2579.

Burkhardt, L., Holzwarth, M., Plietker, B., Bauer, M., 2017. Detection and characterization of hydride ligands in iron complexes by high-resolution hard X-ray spectroscopy and implications for catalytic processes. Inorg. Chem. 56, 13300–13310.

Sedransk Campbell, K.L., Yu, L.C.Y., Williams, D.R, 2017. Siderite corrosion protection for carbon steel infrastructure in post-combustion capture plants. Int. J. Greenhouse Gas Control 58, 232–245.

Cozzi, L. (International E. A. & Gould, T. (International E. A. World Energy Outlook 2021. 1–386 (2021).

Clouse, R. C., Asperger, R. G., 1978. Inhibitor for gas conditioning solutions. United States Patent, 4102804.

Cutsail, G.E., et al., 2020. High-resolution iron X-ray absorption spectroscopic and computational studies of non-heme diiron peroxo intermediates. J. Inorg. Biochem. 203, 110877.

Desimone, M.P., Gordillo, G., Simison, S.N., 2011. The effect of temperature and concentration on the corrosion inhibition mechanism of an amphiphilic amido-amine in CO2 saturated solution. Corros. Sci. 53, 4033–4043.

Diaz-Moreno, S., et al., 2018. The spectroscopy village at diamond light source. J. Synchrotron Radiat. 25, 998–1009.

DuPart, M. S., Bacon, T. R., Edwards, 1993. Understanding corrosion in alkanolamine gas treating plants: Part 2. https://www.osti.gov/biblio/6295319.

DuPart, M. S., Oakes, B. D., Cringle, D. C., 1984. Method and compositions for reducing corrosion in the removal of acidic gases from gaseous mixtures. United States Patent 4446119, 2–5. https://www.osti.gov/biblio/6295319.

Gunasekaran, P., Veawab, A., Aroonwilas, A., 2013. Corrosivity of single and blended amines in CO_2 capture process. Energy Procedia 37, 2094–2099.

Hasib-Ur-Rahman, M., Larachi, F., 2013. Prospects of using room-temperature ionic liquids as corrosion inhibitors in aqueous ethanolamine-based CO2 capture solvents. Ind. Eng. Chem. Res. 52, 17682–17685.

Haszeldine, S.R., 2009. Carbon capture and storage: How green can black be? Science (1979) 325, 1647–1652.

Henson, E. R., Masterson, T. T., Courtwright, J. G., 1986. Corrosion inhibitors for alkanolamines. United States Patent 4595723.

Holoman, J., Asperger, S., Krawczyk, L. S., 1978. Gas scrubbing system. United States Patent (4096085).

Jones, L. W., Alkire, J. D., 1985. Corrosion inhibitor for amine gas sweetening systems. United States. Patent 4541946, 0–5.

Khatri, R.A., Chuang, S.S.C., Soong, Y., Gray, M., 2006. Thermal and chemical stability of regenerable solid amine sorbent for CO_2 capture. Energy Fuel. 20, 1514–1520.

Kittel, J., et al., 2009. Corrosion in MEA units for CO_2 capture: Pilot plant studies. Energy Procedia 1, 791–797.

Kohl, A.L., Nielsen, R.B., 1997. Chapter 2 - Alkanolamines for Hydrogen Sulfide and Carbon Dioxide Removal. In: Kohl, A.L., Nielsen, R.B (Eds.), Gas Purification (Fifth Edition). Gulf Professional Publishing, pp. 40–186. doi:10.1016/B978-088415220-0/50002-1.

Lafuerza, S., et al., 2020. New reflections on hard X-ray photon-in/photon-out spectroscopy. Nanoscale 12, 16270–16284.

MacDowell, N., et al., 2010. An overview of CO_2 capture technologies. Energy Environ. Sci. 3, 1645–1669.

Mago, B. F., West, C. W., 1976. Corrosion inhibitors for alkanolamine gas treating system. United States Patent (3959170).

McCullough, J. G., Barr, K. J., 1985. Corrosion inhibitors for alkanolamine gas treating systems. United States Patent 4502979, 99.

Mondal, M.K., Balsora, H.K., Varshney, P., 2012. Progress and trends in CO_2 capture/separation technologies: A review. Energy 46, 431–441.

Nieh, E.D.Y., 1983. Vanadium-amine corrosion inhibitor system for sour gas conditioning solutions.United States. Patent 4372873.

Oakes, B. D., DuPart, M. S., Cringle, D. C., 1984. Bismuth inhibitors for acid gas conditioning solutions, 4452764. United States Patent.

Pappas, D.K., et al., 2019. Understanding and Optimizing the Performance of Cu-FER for The Direct CH_4 to CH_3OH Conversion. ChemCatChem 11, 621–627.

Parlett, C.M.A., et al., 2014. Alumina-grafted SBA-15 as a high performance support for Pd-catalysed cinnamyl alcohol selective oxidation. Catal. Today 229, 46–55.
Rochelle, G.T., 2009. Amine Scrubbing for CO_2 Capture. Science (1979) 325, 1652–1654.
Sadeek, S.A., Williams, D.R., Sedransk Campbell, K.L., 2018. Using sodium thiosulphate for carbon steel corrosion protection against monoethanolamine and 2-amino-2-methyl-1-propanol. Int. J. Greenhouse Gas Control 78, 125–134.
Saiwan, C., Supap, T., Idem, R.O., Tontiwachwuthikul, P.Part, 2011. 3: Corrosion and prevention in post-combustion CO_2 capture systems. Carbon Management 2, 659–675.
Soosaiprakasam, I.R., Veawab, A., 2008. Corrosion and polarization behavior of carbon steel in MEA-based CO_2 capture process. Int. J. Greenhouse Gas Control 2, 553–562.
Soosaiprakasam, I.R., Veawab, A., 2009. Corrosion inhibition performance of copper carbonate in MEA- CO_2 capture unit. Energy Procedia 1, 225–229.
Srinivasan, S., Veawab, A., Aroonwilas, A., 2013. Low toxic corrosion inhibitors for amine-based CO_2 capture process. Energy Procedia 37, 890–895.
Stowe, H.M., Hwang, G.S., 2017. Fundamental Understanding of CO_2 Capture and Regeneration in Aqueous Amines from First-Principles Studies: Recent Progress and Remaining Challenges. Ind. Eng. Chem. Res. 56, 6887–6899.
Thitakamol, B., Veawab, A., 2008. Foaming behavior in CO_2 absorption process using aqueous solutions of single and blended alkanolamines. Ind. Eng. Chem. Res. 47, 216–225.
Uhlig, H.H., Revie, R.W., 2008. Corrosion and Corrosion Control: An Introduction to Corrosion Science and Engineering. A John Wiley and Sons, INC., publication.
Veawab, A., Tontiwachwuthikul, P., Bhole, S.D., 1997. Studies of Corrosion and Corrosion Control in a CO_2-2-Amino-2-methyl-1-propanol (AMP) Environment. Ind. Eng. Chem. Res. 36, 264–269.
Veawab, A., Tontiwachwuthikul, P., Chakma, A., 2001. Investigation of low-toxic organic corrosion inhibitors for CO_2 separation process using aqueous MEA solvent. Ind. Eng. Chem. Res. 40, 4771–4777.
Vollmers, N.J., et al., 2016. Experimental and theoretical high-energy-resolution X-ray absorption spectroscopy: Implications for the investigation of the entatic state. Inorg. Chem. 55, 11694–11706.
Wu, X., Yu, Y., Qin, Z., Zhang, Z., 2014. The advances of post-combustion CO_2 capture with chemical solvents: Review and guidelines. Energy Procedia 63, 1339–1346.
Xiang, Y., Yan, M., Choi, Y.S., Young, D., Nesic, S., 2014. Time-dependent electrochemical behavior of carbon steel in MEA-based CO_2 capture process. Int. J. Greenhouse Gas Control 30, 125–132.
Yu, L.C.Y., 2015. Investigating the Corrosion and Surface Passivation of Carbon Steel in Novel Amine Plants. Imperial College London.
Zheng, L., et al., 2016. Understanding the corrosion of CO_2-loaded 2-amino-2-methyl-1-propanol solutions assisted by thermodynamic modeling. Int. J. Greenhouse Gas Control 54, 211–218.
Zheng, L., Landon, J., Koebcke, N.C., Chandan, P., Liu, K., 2015. Suitability and Stability of 2-Mercaptobenzimidazole as a Corrosion Inhibitor in a Post-Combustion CO_2 Capture System. Corrosion 71, 692–702.
Zheng, L., Landon, J., Matin, N.S., Liu, K., 2016. $FeCO_3$ coating process toward the corrosion protection of carbon steel in a postcombustion CO_2 capture system. Ind. Eng. Chem. Res. 55, 3939–3948.
Pearce, Wolcott, R. A. & Pauley, C. R. United States Patent (4440731). (1984).